IEEE Access
Multidisciplinary | Rapid Review | Open Access Journal

Received March 17, 2020, accepted March 31, 2020, date of publication April 3, 2020, date of current version April 20, 2020.

Digital Object Identifier 10.1109/ACCESS.2020.2985415

Design of a Microstrip Three-State Switchable and Fully Tunable Bandpass Filter With an Extra-Wide Frequency Tuning Range

CHI-FENG CHEN, (Member, IEEE)
Department of Electrical Engineering, Tunghai University, Taichung 40704, Taiwan
e-mail: cfchen@thu.edu.tw

This work was supported by the Ministry of Science and Technology, Taiwan, under Grant MOST 107-2221-E-029-009 and Grant MOST 108-2221-E-029-001.

ABSTRACT In this study, a new method and structure are proposed to design of a switchable and fully tunable microstrip bandpass filter (BPF). The central frequency and bandwidth (or the resonance frequency of the resonators, coupling coefficient between resonators, and external quality factor of the I/O resonator) of the proposed BPF can be efficiently controlled using varactor diodes as tuners. In addition, the proposed BPF is designed to have three operating states, each with a different frequency tuning range. The three operating states can be switched between independently by introducing three pairs of switching diodes in the input and output feeding structures. Because of the ability to switch among the three operating states, an extra-wide frequency tuning range can be achieved. For demonstration, a two-pole switchable and tunable BPF was designed and implemented using microstrip technology. The experimental and simulation results were consistent and indicate that a wide frequency tuning range from 0.54 to 2.4 GHz, corresponding to a fractional tuning range of 127%, and a nearly constant absolute bandwidth of 82 MHz are achieved. In addition, the proposed switchable and tunable BPF is small ($0.24\lambda_g \times 0.15\lambda_g$).

INDEX TERMS Bandpass filter (BPF), microstrip filter, switchable filter, tunable filter.

I. INTRODUCTION

In modern RF and microwave communication systems, electronically tunable filters play a crucial role. These tunable filters are often required to achieve frequency tuning, bandwidth tuning, or transmission zero (TZ) tuning. Numerous planar RF and microwave bandpass filters (BPFs) have been investigated and successfully developed using various advanced techniques [1]–[24].

In [1] and [2], reconfigurable microstrip BPFs based on varactor-tuned dual-mode open-loop resonators were proposed. By suitably changing the even- and odd-mode resonance frequencies of the dual-mode open-loop resonator, passband frequency tuning can be accomplished. In [3], a tunable microstrip BPF with a pair of controllable TZs was developed. The central frequency, bandwidth, and TZs of the BPF can be tuned by introducing two pairs of varactor diodes connected at the open ends of each coupled resonator. In [4] and [5], tunable microstrip combline BPFs were presented. A short transmission line between two adjacent resonators and two pairs of varactor diodes located between two coupled resonators were employed for bandwidth tuning. In [6], a tunable microstrip BPF with a constant absolute bandwidth (CABW) was proposed to enlarge the frequency tuning range by using a combline resonator loaded with lumped series resonators. In [7], a two-pole microstrip BPF with tunable central frequency, bandwidth, and TZs was investigated. The interstage coupling strength was controlled using the T-type bandwidth control circuit proposed in the study, and the I/O coupling strength and locations of the two generated TZs were controlled using a back-to-back varactor set. In [8], a two-pole microstrip tunable dual-mode BPF with a constant fractional bandwidth (CFBW) was proposed. The major contribution of [8] was capability for I/O external quality factor control. By introducing two varactor diodes located at the open ends of the feeding coupled lines and suitably adjusting their respective capacitance, the I/O external quality factor can be fixed over the frequency tuning range, and thus, a CFBW-tunable BPF can be implemented.In [9], a wideband tunable microstrip

The associate editor coordinating the review of this manuscript and approving it for publication was Feng Lin.

BPF was developed using varactor-loaded stepped-impedance resonators (SIRs).

The length ratio of the varactor-loaded SIR was optimized to obtain a large frequency tuning range. In [10], a tunable four-pole four-TZ microstrip BPF was proposed. The cross-coupling and source-load coupling techniques were used to generate the four TZs. In addition, by adjusting the magnetic and electric coupling strengths, a CFBW could be realized. In [11], a tunable microstrip BPF using varactor-loaded short-circuited coupled lines was proposed. By suitably locating three pairs of varactor diodes in the short-circuited coupled lines, the central frequency, bandwidth, and TZ of the BPF could be efficiently controlled. In [12], a CABW tunable microstripBPF consisting of two varactor-loaded nonuniform quarter-wave spiral resonators was investigated. The tunable selectivity and tunable passband were achieved by controlling the inherent TZs, which were generated by a combline coupled section. In [13], a CABW tunable microstrip BPF based on a half-wavelength resonator with a center-tapped open-stub was proposed. By controlling the in-band transmission poles, a CFBW could be achieved. In [14]–[17], tunable microstrip BPFs based on switchable varactor-tuned resonators were proposed. Because these BPFs were designed to switch between low-band and high-band tuning states, a wide frequency tuning range with a CABW was achieved. However, due to the structure limitation, the designs are difficult to realize more operating states with a wider frequency tuning range. In [18], a CABW tunable microstrip BPF with two self-adaptive TZs was presented. Frequency-dependent S–L coupling was achieved to produce two TZs at the lower and upper sides of the passband, which led to higher selectivity. Numerous systematic design methodologies for higher-order tunable microstrip BPFs are provided in [19]–[23]. In addition, a switchable single-band or dual-band tunable microstrip BPF based on synchronously tuned dual-mode resonators was explored in [24].

The rapid development of RF and microwave communication technology has led to increasing demand for tunable and reconfigurable BPFs with wide frequency tuning ranges. However, the fractional frequency tuning ranges for most of the abovementioned tunable BPFs are $< 70\%$. In this study, a new method is proposed to design a tunable microstrip BPF with an extra-wide frequency tuning range (127%). The proposed BPF is designed to operate in three tuning states with a continuous frequency tuning range. The BPF can switch between the three tuning states; therefore, an extra-wide frequency tuning range with a CABW is achieved. Full-wave electromagnetic (EM) simulation and measurements were used to validate a design example.

This paper is organized as follows. In Section 2, the detailed procedure for designing the switchable and tunable microstrip BPF is presented. The theoretical analysis and experimental treatment are also included. In Section 3, a CABW switchable and tunable BPF is implemented using microstrip technology to validate the feasibility of the proposed idea. The measurement results are presented and compared with the full-wave EM simulation results. In addition, the performance is compared with that of the reported tunable BPFs, and the new academic contributions of the proposed BPF are highlighted. Finally, the conclusion is presented in Section 4.

II. CIRCUIT DESIGN

Fig. 1(a) presents a design concept of the proposed three-state switchable and tunable BPF. The BPF is designed to have three operating states, each with a different frequency tuning range. The frequency tuning ranges for states I, II, and III are f_{01}^{I}–f_{02}^{I}, f_{01}^{II}–f_{02}^{II}, and f_{01}^{III}–f_{02}^{III}, respectively; f_{02}^{I} and f_{02}^{II} are close to f_{01}^{II} and f_{01}^{III}, respectively. Because of the ability to switch among the three operating states, a wide continuous frequency tuning range (from f_{01}^{I} to f_{02}^{III}) is achieved. The realizable coupling structure of the proposed N-pole switchable and tunable BPF is presented in Fig. 1(b), with each node representing a vector-tuned resonator and S and L being the source and load, respectively. The passband of state n is formed by the resonators 1^n to N^n (n = I, II, and III). The passband of each operating state is realized through an independent coupling path; therefore, the structure has many degrees of design freedom. Note that, there will be a tradeoff between the number of operating states and circuit size in this design. In addition, the central frequencies and bandwidths of all passbands for the three operating states can be flexibly controlled.

Normally, increasing the filter order will result in a larger in-band insertion loss and a larger circuit size for practical implementation. Thus, taking into consideration of the insertion loss and circuit size, the BPF was then designed to have a two-pole filtering response, as shown in Fig. 1(c), for a demonstration. Because the passband of each operating state is realized using an independent coupling path, each single-state tunable BPF can be designed individually. Fig. 2(a) presents the circuit model of a two-pole single-state tunable BPF. The BPF consists of a pair of varactor-loaded quarter-wavelength resonators. The equivalent circuit model of a varactor-loaded resonator is presented in Fig. 3. A varactor (C_f) for frequency tuning is connected at the open resonator end. The input admittance (Y_{in1}; labeled in Fig. 3) can be obtained using

$$Y_{in1} = j\left(\omega C_f - \frac{\cot\theta_R}{Z_R}\right) \tag{1}$$

The resonance condition of the varactor-loaded resonator can be obtained using

$$\mathrm{Im}\,[Y_{in1}] = 0 \tag{2}$$

Thus, the varactor capacitance (C_f) can be used to control the resonant frequency of the varactor-loaded resonator, except for the characteristic impedance (Z_R) and electrical length (θ_R).

In addition, to achieve bandwidth tuning, both the coupling coefficient and I/O external quality factor should be controlled. To achieve this, a pair of varactors (C_m) are placed

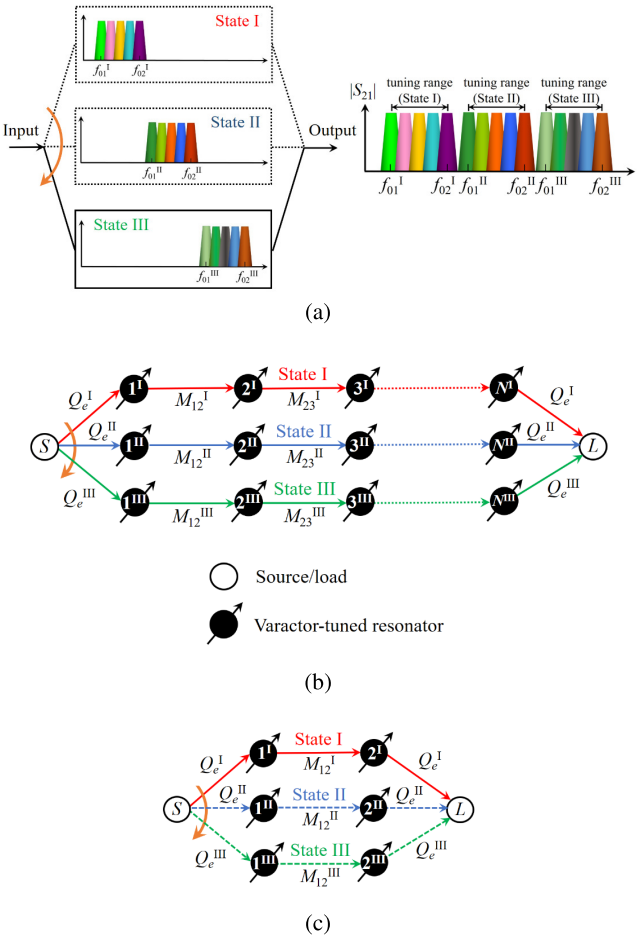

FIGURE 1. Proposed three-state switchable and tunable BPF. (a) Design concept. (b) Coupling scheme for N-pole filtering response. (c) Coupling scheme for 2-pole filtering response.

between the coupled resonators, as illustrated in Fig. 2(a), and are employed to control the coupling coefficient. To facilitate analysis, the equivalent circuit model of the coupled resonators is presented in Fig. 4(a). Because of the symmetric nature of the circuit model, even–odd mode analysis can be adopted. The corresponding even-mode and odd-mode equivalent circuits are presented in Figs. 4(b) and (c), respectively. The even-mode and odd-mode input admittances—that is, $Y_{in,e}$ and $Y_{in,o}$, in the half circuits in Figs. 4(b) and (c), respectively—can be obtained as follows:

$$Y_{in,e} = j\omega C_f + Y_{0,e}\frac{Y_{L,e} + jY_{0,e}\tan\theta_{R1}}{Y_{0,e} + jY_{L,e}\tan\theta_{R1}} \tag{3}$$

$$Y_{in,o} = j\omega C_f + Y_{0,o}\frac{Y_{L,o} + jY_{0,o}\tan\theta_{R1}}{Y_{0,o} + jY_{L,o}\tan\theta_{R1}} \tag{4}$$

$$Y_{L,e} = -jY_{0,e}\cot\theta_{R2} \tag{5}$$

$$Y_{L,o} = j\omega C_m - jY_{0,o}\cot\theta_{R2} \tag{6}$$

where $Y_{0,e}$ and $Y_{0,o}$ are the even-mode and odd-mode characteristic admittances of the coupled lines, respectively. Therefore, the coupling coefficient M can be derived in terms of

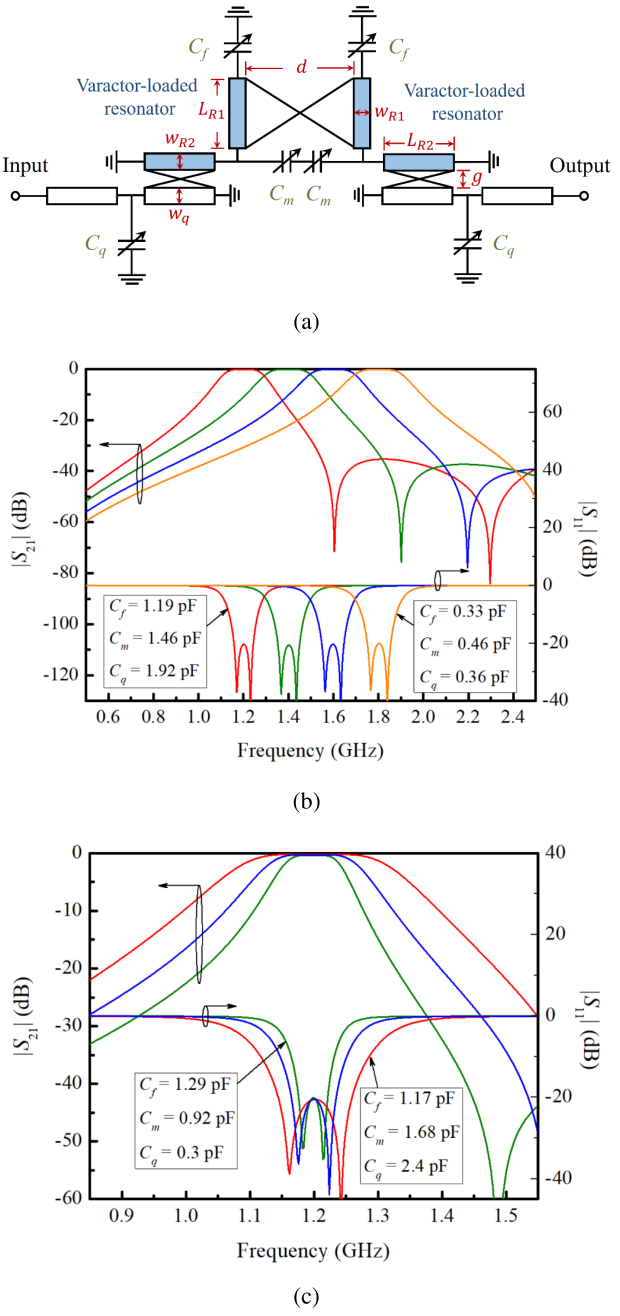

FIGURE 2. (a) Circuit model of a two-pole single-state tunable BPF. (b) Simulated results of the BPF with tunable central frequencies. (c) Simulated results of the BPF with tunable bandwidths. ($L_{R1} = L_{R2} =$ 10 mm, $w_{R1} = w_{R2} = w_q = 1$ mm, $d = 4.2$ mm, and $g = 0.58$ mm).

$Y_{in,e}$ and $Y_{in,o}$ as follows:

$$M = \frac{\mathrm{Im}\left[Y_{in,e}(\omega_0) - Y_{in,o}(\omega_0)\right]}{2b} \tag{7}$$

$$b = \frac{\omega_0}{2}\frac{\partial}{\partial\omega}\left\{\mathrm{Im}\left[\frac{Y_{in,e} - Y_{in,o}}{2}\right]\right\}\Bigg|_{\omega_0} \tag{8}$$

where ω_0 denotes the resonant frequency. Based on this analysis, the varactor capacitance C_m clearly controls the coupling coefficient.

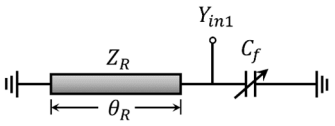

FIGURE 3. Equivalent-circuit model of the varactor-loaded resonator.

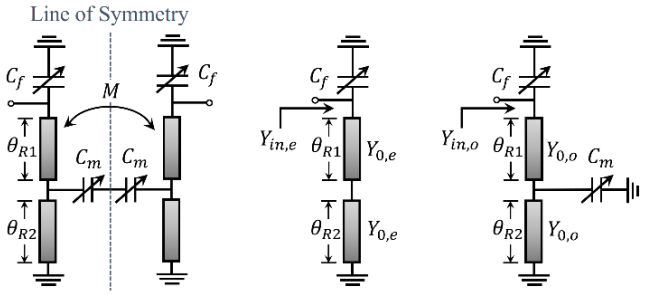

FIGURE 4. Equivalent-circuit model of coupled resonators in Fig. 3(a) and its (b) even-mode and (c) odd-mode circuits.

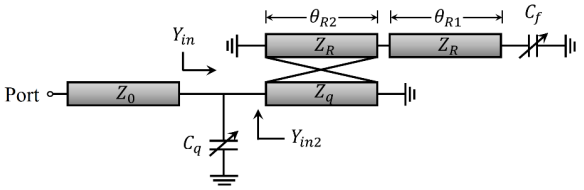

FIGURE 5. Equivalent-circuit model of the resonator with an external coupled-line circuit.

For the I/O external quality factor control, a pair of varactors (C_q) are loaded at the input and output coupled lines of the BPF, as shown in Fig. 2(a). The equivalent circuit model of the varactor-loaded resonator with an external coupled-line circuit is presented in Fig. 5. The input admittance Y_{in} observed on the feeding line (labeled in Fig. 5) can be obtained as follows:

$$Y_{in} = i\omega C_q + Y_{in2} \tag{9}$$

Then, the I/O external quality factor can be calculated as follows:

$$Q_e = \frac{\omega_0 Z_0}{2} \frac{\partial \mathrm{Im}\left[Y_{in}\left(\omega_0\right)\right]}{\partial \omega} \tag{10}$$

Thus, the varactor capacitance C_q can control the I/O external quality factor. Figs. 2(b) and (c) present the simulated performance of the circuit model for a two-pole single-state tunable BPF. The central frequency and bandwidth of the BPF can be efficiently controlled by suitably adjusting the varactor capacitances C_f, C_m, and C_q. In addition, an extra TZ is produced and located at the upper side of the passband due to the property of the I/O parallel coupled-line section [25].

For demonstration, a two-pole three-state switchable and tunable BPF was designed and implemented on a Rogers

TABLE 1. Filter specification.

	State-I	State-II	State-III
Central frequency (GHz)	0.54–1	1–1.6	1.6–2.4
Bandwidth (MHz)	82	82	82
Fractional bandwidth (%)	15–8.2	8.2–5	5–3.4
Filter order	2	2	2
Response	Chebyshev (0.04321 dB ripple)		

RO4003 substrate with relative dielectric constant and thickness of 3.38 and 1.524 mm, respectively. The design specification of the BPF is presented in Table 1. The microstrip configuration of the proposed two-pole three-state switchable and tunable BPF is presented in Fig. 6. The proposed three-state switchable and tunable BPF consists of three pairs of varactor-loaded quarter-wavelength resonators that operate in different frequency ranges. The varactor capacitances C_{f1}, C_{m1}, and C_{q1} (tuned by the bias voltages V_{f1}, V_{m1}, and V_{q1}, respectively) are used to control the central frequency f_0^I, coupling coefficient M_{12}^I, and external quality factor Q_e^I, respectively, for state I operation; the varactor capacitances C_{f2}, C_{m2}, and C_{q2} (tuned by the bias voltages V_{f2}, V_{m2}, and V_{q2}, respectively) are used to control the central frequency f_0^{II}, coupling coefficient M_{12}^{II}, and external quality factor Q_e^{II}, respectively, for state II operation; and finally, the varactor capacitances C_{f3}, C_{m3}, and C_{q3} (tuned by the bias voltages V_{f3}, V_{m3}, and V_{q3}, respectively) are used to control the central frequency f_0^{III}, coupling coefficient M_{12}^{III}, and external quality factor Q_e^{III}, respectively, for state III operation. In addition, three pairs of switching diodes (D_1, D_2, and D_3) controlled by the bias voltages V_{d1}, V_{d2}, and V_{d3}, respectively, are connected to the T-junctions of the input and output coupled lines to achieve the state switching feature. Simplified circuits of the proposed switchable and tunable BPF for states I, II, and III are shown in Figs. 7(a), (b), and (c), respectively. As D_1 is turned on (that is, enters the forward-biased state) and D_2 and D_3 are turned off (that is, enter the reverse-biased state), the BPF switches to state I operation (see Fig. 7(a)). As D_2 is turned on and D_1 and D_3 are turned off, the BPF switches to state II operation (see Fig. 7(b)). As D_3 is turned on and D_1 and D_2 are turned off, the BPF switches to state III operation (see Fig. 7(c)).

Fig. 8 depicts the resonance frequencies as a function of the varactor capacitance (C_f). Resonance frequencies of resonator $1^{\mathrm{I}}/2^{\mathrm{I}}$ ranging from 1 to 0.54 GHz are achieved when C_{f1} is varied from 0.3 to 2.4 pF and the resonator length l_1 is determined to be 35.6 mm. Resonance frequencies of resonator $1^{\mathrm{II}}/2^{\mathrm{II}}$ ranging from 1.78 to 0.96 GHz are achieved when C_{f2} is varied from 0.3 to 2.4 pF and the resonator length l_5 is determined to be 20 mm. The resonance frequencies of resonator $1^{\mathrm{III}}/2^{\mathrm{III}}$ ranging from 2.7 to 1.3 GHz are achieved when C_{f3} is varied from 0.3 to 2.4 pF and the resonator length l_{10} is determined to be 11 mm. In summary, the frequency tuning ranges of all resonators satisfy the required design specification (Table 1).

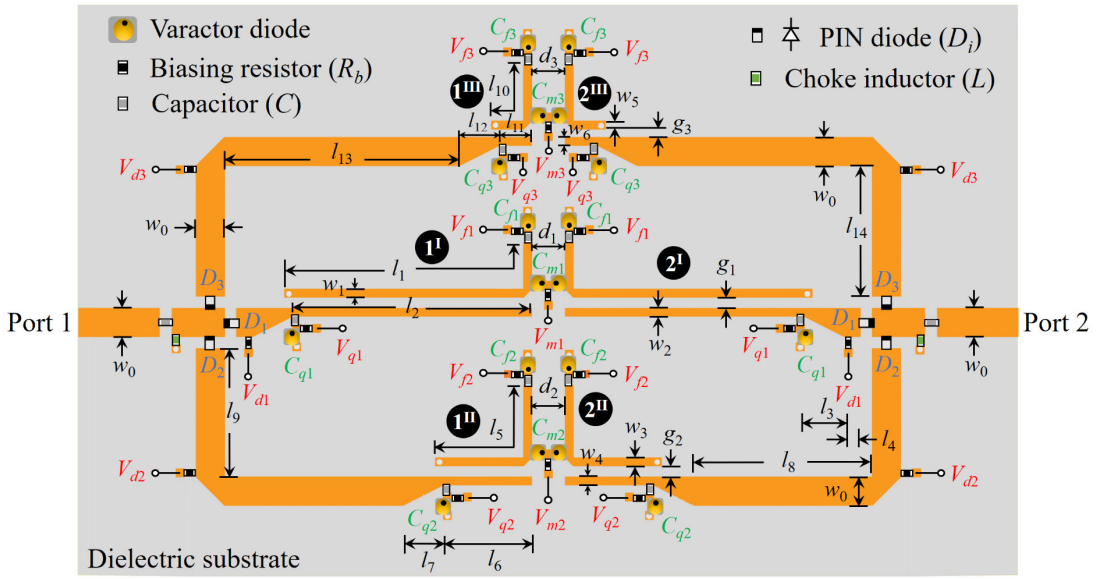

FIGURE 6. Microstrip configuration of the proposed switchable and tunable BPF.

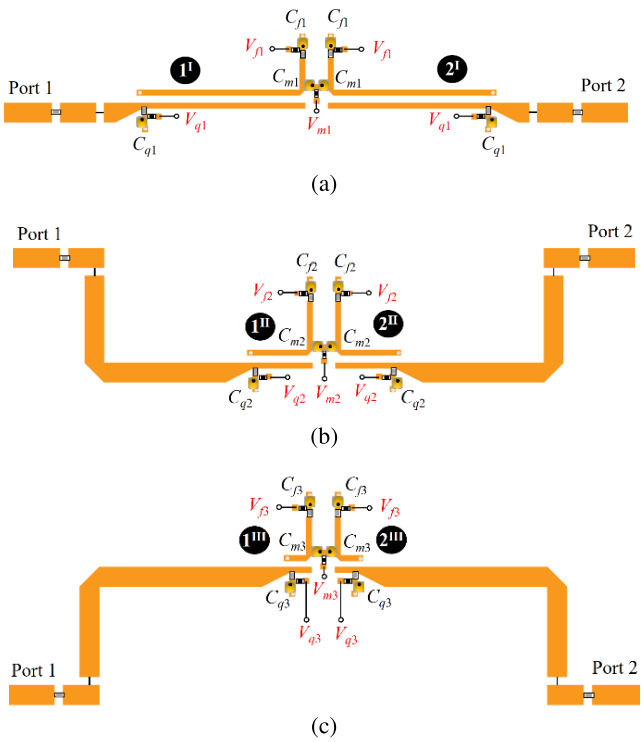

FIGURE 7. Simplified circuits of the proposed switchable and tunable BPF for (a) state I operation, (b) state II operation, and (c) state III operation.

The theoretical values of the coupling coefficient and external quality factor can be calculated as follows [25]:

$$M = \frac{\Delta}{\sqrt{g_1 g_2}} \tag{11}$$

$$Q_e = \frac{g_0 g_1}{\Delta} \tag{12}$$

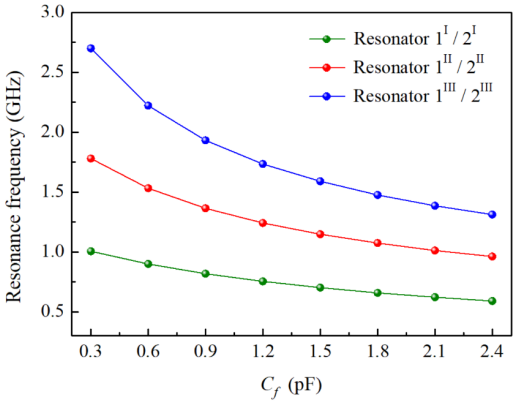

FIGURE 8. Resonance frequency against C_f. ($l_1 = 35.6$ mm, $l_5 = 20$ mm, $l_{10} = 11$ mm, and $w_1 = w_3 = w_5 = 1$ mm).

where Δ and g denote the fractional bandwidth and lumped element values of a low-pass prototype filter, respectively. After a passband ripple of 0.04321 dB is selected, the corresponding g-values are found to be $g_0 = 1$, $g_1 = 0.6648$, and $g_2 = 0.5445$ [26].

The coupling coefficient can be extracted from the coupled-resonator configuration using the following formula [25]:

$$M = \frac{f_{p2}^2 - f_{p1}^2}{f_{p2}^2 + f_{p1}^2} \tag{13}$$

where f_{p1} and f_{p2} are the lower and higher fundamental resonance frequencies of two adjacent coupled resonators, respectively. The design curves of the coupling coefficients for states I, II, and III are plotted in Figs. 9(a), (b), and (c), respectively. A wide range of coupling

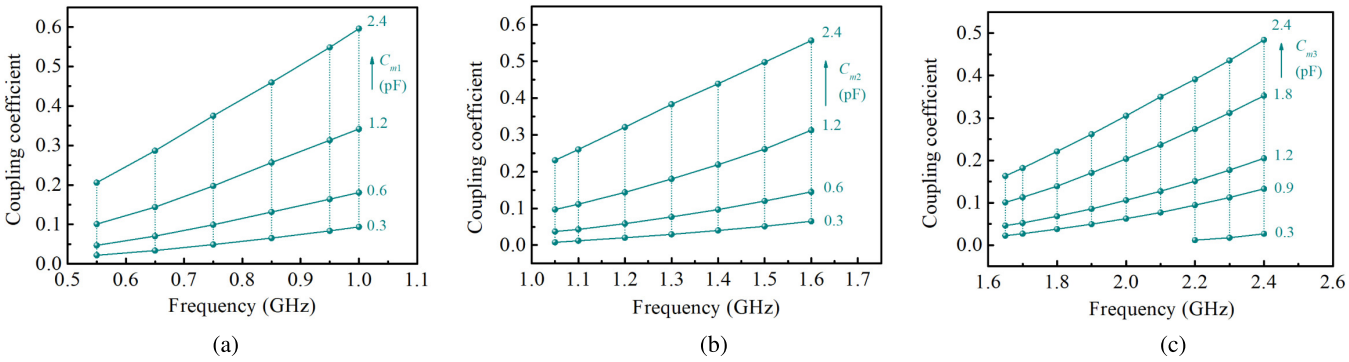

FIGURE 9. Extracted coupling coefficients as a function of resonance frequency. (a) State-I, (b) state-II, and (c) state-III. ($d_1 = d_2 = d_3 = 4.2$mm).

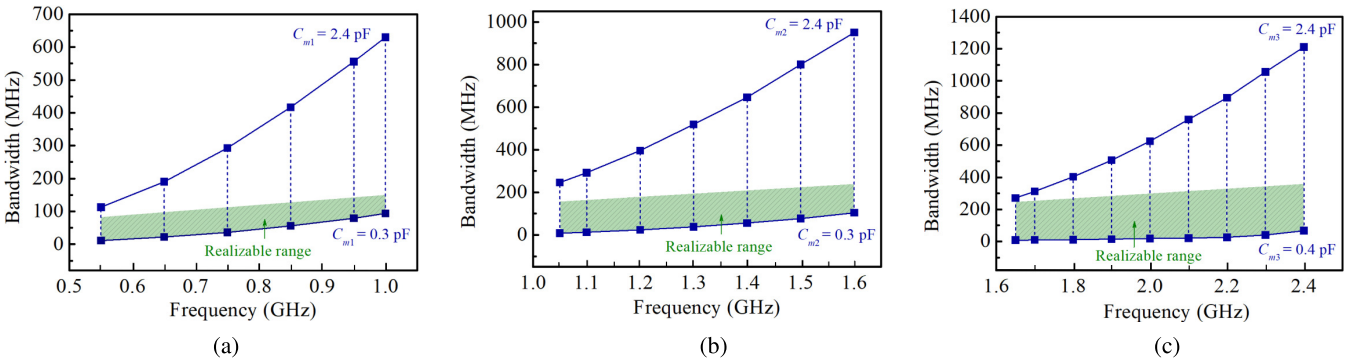

FIGURE 10. 1-dB tunable bandwidth versus frequency. (a) State-I, (b) state-II, and (c) state-III. ($d_1 = d_2 = d_3 = 4.2$mm).

coefficients can be realized when C_m is varied from 0.3 to 2.4 pF. Figs. 10(a), (b), and (c) present the corresponding 1-dB tunable bandwidth versus frequency for states I, II, and III, respectively. Due to the design method based on the coupled-resonator technique is applicable only to the design of a narrowband BPF ($\Delta \leq 15\%$) and, therefore, the shaded regions in Figs. 10(a), (b), and (c) are the realizable bandwidth range; however, it still includes the desired bandwidth specification in Table 1.

The I/O external quality factor can be extracted from a resonator with an external coupled-line circuit and the following equation [25]:

$$Q_e = \frac{\pi f_0 \tau_d (f_0)}{2} \tag{14}$$

where $\tau_d (f_0)$ denotes the group delay at central frequency f_0. The extracted and theoretical external quality factors with a CABW of 82 MHz for states I, II, and III are plotted in Figs. 11(a), (b), and (c), respectively. By suitably adjusting the varactor capacitance C_q, the extracted values of the external quality factor are found to be favorably consistent with the theoretical values. Fig. 12 shows the theoretical and EM simulated frequency responses of the switchable and tunable BPF. Note that, the losses from the varactors, switching diodes, and materials are considered in the EM simulations. Obviously, the EM simulated frequency responses are in reasonable agreement with the theoretical ones.

The procedure of designing the proposed switchable and tunable BPF is summarized as follows.

Step 1) Establish the specifications, including the central frequency, passband bandwidth, filter order, and frequency response.

Step 2) Determine the structural parameters of the varactor-loaded quarter-wavelength resonators (l_1, l_5, l_{10}, w_1, w_3, and w_5) to satisfy the required frequency tuning range.

Step 3) Evaluate the theoretical values of the coupling coefficients (M_{12}^I, M_{12}^{II}, and M_{12}^{III}) and I/O external quality factors (Q_e^I, Q_e^{II}, and Q_e^{III}) by using (11) and (12).

Step 4) Extract the coupling coefficients and I/O external quality factors from the filter structure by using (13) and (14). Then, the distances between the adjacent resonators (d_1, d_2, and d_3) and physical parameters of the I/O feeding structure (g_1, g_2, g_3, w_2, w_4, and w_6) can be determined when the extracted values of coupling coefficients and external quality factors are consistent with the theoretical values. In addition, by loading the varactors C_{m1}, C_{m2}, C_{m3}, C_{q1}, C_{q2}, and C_{q3} into the filter structure, the bandwidth tuning can be achieved.

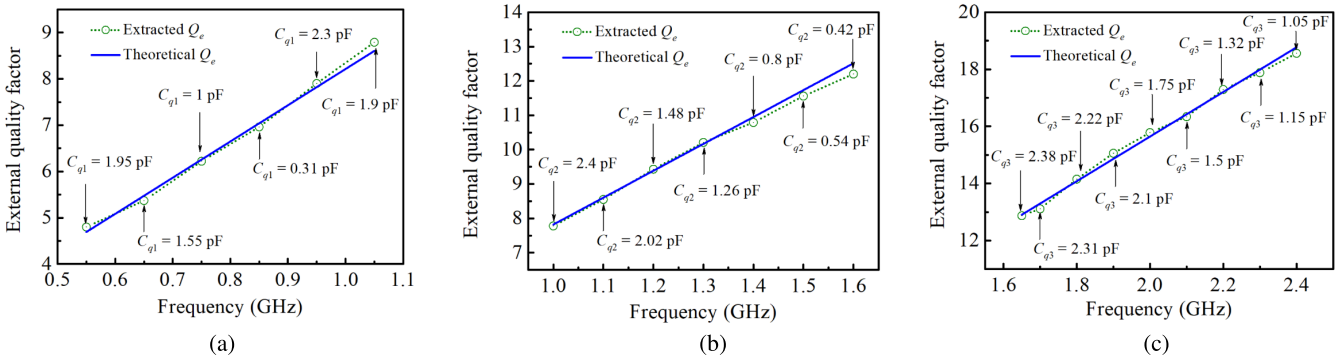

FIGURE 11. Extracted external quality factors as a function of resonance frequency. (a) State-I, (b) state-II, and (c) state-III. ($g_1 = g_2 = 0.38$mm, $g_3 = 0.1$mm, and $w_2 = w_4 = w_6 = 1$ mm).

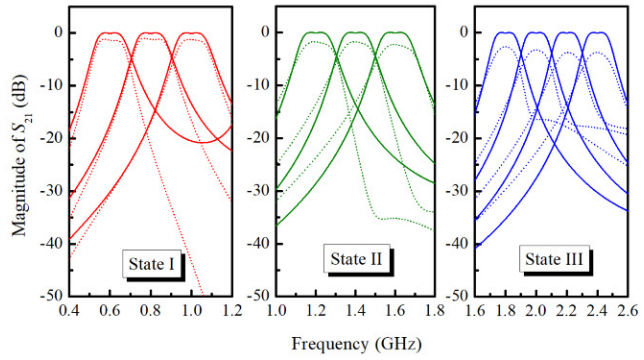

FIGURE 12. Theoretical (solid curves) and EM simulated (dotted curves) frequency responses of the switchable and tunable BPF.

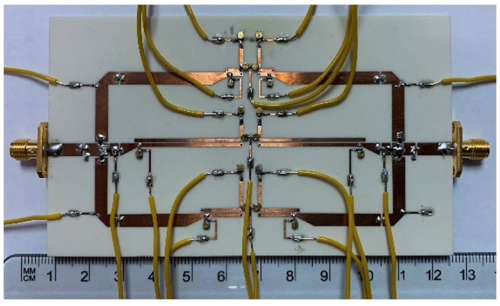

FIGURE 13. Picture of the fabricated switchable and tunable BPF.

Step 5) Add three pairs of p-i-n diodes (D_1, D_2, and D_3) to the T-junctions of the input and output coupled lines to achieve the state switching feature.

Step 6) Perform optimization to acquire the desired pass-band performance (if required).

III. EXPERIMENTAL VALIDATION

Fig. 13 presents a photograph of the fabricated switchable and tunable BPF. The dimensions of the fabricated BPF are detailed in Table 2, and its overall circuit area is $0.24\lambda_g \times 0.15\lambda_g$ (i.e., 87.8×55.3 mm^2), where λ_g is the guided wavelength at the lowest operating frequency (i.e., 0.54 GHz).

TABLE 2. Dimensions of the proposed switchable and tunable BPF. (Unit: mm).

l_1	l_2	l_3	l_4	l_5	l_6	l_7
35.6	29.8	5	3	20	11	5
l_8	l_9	l_{10}	l_{11}	l_{12}	l_{13}	l_{14}
22.3	16	11	4	5	29.3	16.3
w_0	w_1	w_2	w_3	w_4	w_5	w_6
3.53	1	1	1	1	1	1
d_1	d_2	d_3	g_1	g_2	g_3	
4.2	4.2	4.2	0.38	0.38	0.1	

Several lumped components are employed for bypass capacitors ($C = 33$ pF), choke inductors ($L = 220$ nH), and biasing resistors ($R_b = 10$ kΩ, which is utilized to limit the bias current). In this design, all varactors are realized using MA46H201 GaAs diodes with capacitance tuning in the range 0.3–2.4 pF for bias in the range 0.4–18 V [27]. The switching diodes are realized using Infineon BRA65-02V p-i-n diodes and can be turned on by applying a bias voltage of 1 V [28].

The full-wave EM simulation is performed using Keysight Advanced Design System (ADS), and measurement is accomplished using the Agilent N5230A network analyzer. The equivalent circuits for varactors [27] and switching diodes [28], [29] were incorporated in the EM simulator to obtain the simulated frequency response. The EM simulated and measured S-parameters ($|S_{11}|$ and $|S_{21}|$) of the fabricated switchable and tunable BPF are presented in Figs. 14(a) and (b), where the solid and dotted lines represent the simulation and measurement results, respectively. Favorable agreement is accomplished between the proposed and simulated model. A wide frequency tuning range from 0.54 to 2.4 GHz (corresponding to a fractional tuning range of 127%) with an approximate CABW of 82 MHz is achieved. The experimental results of the BPF indicate that the return loss (i.e., $-20\log|S_{11}|$) for all three operating states is >15 dB, and the insertion loss (i.e., $-20\log|S_{21}|$) is between 1.8 and

TABLE 3. Comparison with other previous works.

	Frequency range (GHz)	Fractional tuning range (%)	CABW/ CFBW	Filter order	Insertion loss (dB)	Bandwidth control	Number of states	Number of control voltages	Size (λ_g^2)
This work	0.54–2.4	127	CABW (82 MHz)	2	1.8–5.4	Yes	3	12	0.036
[1]	0.86–0.91	5	CABW	2	3.3–4.3	No	N.A.	2	0.013
[2]	0.6–1.07	56	CABW (80 MHz)	2	< 1.8	No	N.A.	1	0.006
[3]	1.4–2	35	CABW (158 MHz)	2	< 4	No	N.A.	2	N.A.
[4]	1.5–2.2	38	CABW (160 MHz)	3	3.1–6.5	Yes	N.A.	3	0.038
[5]	1.55–2.1	30	CABW (80 MHz)	4	4.5–6	No	N.A.	4	0.032
[6]	1.7–2.2	26	CABW (100 MHz)	2	1.6–2	No	N.A.	5	0.189
[7]	1.7–2.7	45	CABW (110 MHz)	2	3.8–4.9	Yes	N.A.	4	0.008
[8]	1.62–1.96	19	CFBW (5%)	2	2.84–2.9	Yes	N.A.	2	0.134
[9]	0.6–1.015	51	N.A.	2	1.1–2.8	No	N.A.	2	0.036
[10]	0.97–1.53	44	CFBW (5.5%)	4	2–4.2	No	N.A.	1	0.009
[11]	0.56–1.15	69	CABW	2	1.4–4.5	Yes	N.A.	4	0.003
[12]	0.9–1.5	50	CABW (290 MHz)	2	1.2–2.3	Yes	N.A.	3	0.004
[13]	0.59–0.88	39	CABW (115 MHz)	2	1.53	Yes	N.A.	7	~0.04
[14]	0.25–0.73	98	CABW (70 MHz)	2	1.6–4.1	Yes	2	6	0.056
[15]	1.1–2.1	63	CABW (40 MHz)	2	4.4–6.1	Yes	2	9	0.016
[16]	0.6–1.71	96	CABW (114 MHz)	2	2.5–4.2	No	2	4	0.005
[17]	0.54–1.8	107	CABW (82 MHz)	3	4–5.4	No	2	6	0.009
[18]	0.43–0.72	50.4	CABW (75 MHz)	2	1.34–2.92	No	N.A.	1	0.022
[19]	0.88–1.12	24	CABW (40.8 MHz)	4	4.8–7.1	No	N.A.	1	0.073
[20]	0.225–0.4	56	CFBW (2.5%)	4	5.6–9.2	No	N.A.	1	N.A.
[21]	0.95–1.48	43.6	CABW (117 MHz)	4	3.5–4.4	No	N.A.	2	0.096
[22]	0.7–1.44	69	CFBW	2	4.4–6.6	Yes	2	10	0.029
[23]	1.25–2.1	51	CFBW (4%)	4	3.5–8.5	Yes	N.A.	5	0.072
[24]	0.76–1.78	80.3	CABW (84 MHz)	2	2–4.5	No	1	1	N.A.

CABW: constant absolute bandwidth; CFBW: constant fractional bandwidth

5.4 dB over the whole frequency tuning range. The insertion loss may be primarily caused by conductor loss and the finite Q-factor of the diodes. Normally, a narrower fractional bandwidth results in a larger in-band insertion loss. Therefore, the insertion losses in state III are higher than those in states I and II as expected. In addition, the input 1-dB compression point of the fabricated switchable and tunable BPF is approximately 14 dBm, and the input third-order

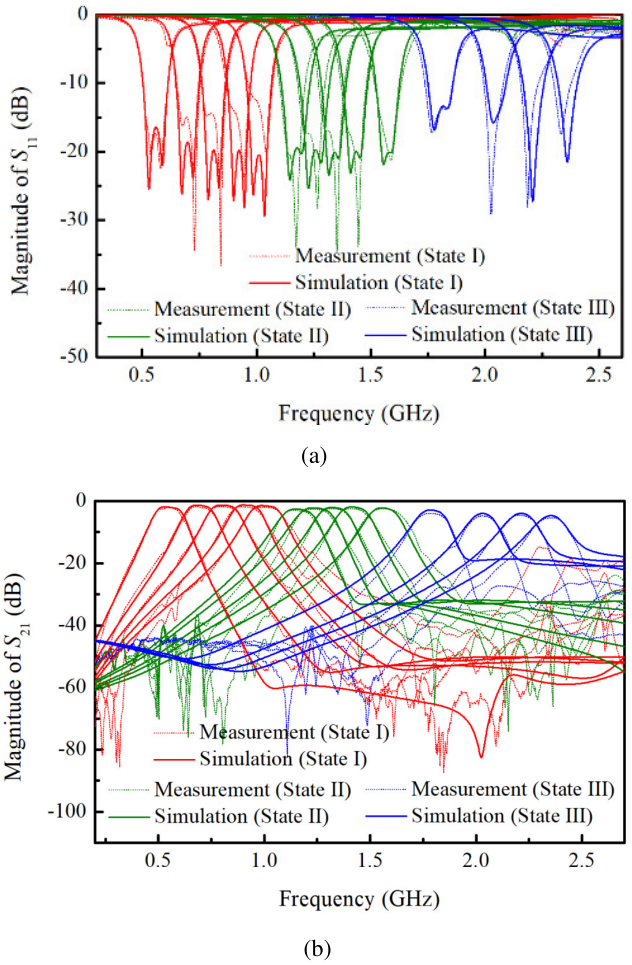

FIGURE 14. Simulation and measurement. (a) $|S_{11}|$ and (b) $|S_{21}|$.

intercept point with the two tones separated by 5 MHz is 16–22 dBm in the whole frequency tuning range.

To highlight the academic contributions of the proposed switchable and tunable BPF, a comparison of the proposed BPF with state-of-the-art tunable BPFs is provided in Table 3. Among the tunable BPFs considered, the proposed BPF has the largest fractional frequency tuning range (i.e., 127%) with an approximate CABW of 82 MHz. In addition, the central frequency and bandwidth of the proposed BPF can be efficiently controlled. The proposed BPF is designed to operate in three states without a considerable increase in size. Additionally, it has a simpler circuit layout and is easier to design. In summary, the proposed BPF has an extra-wide frequency tuning range, flexible frequency and bandwidth control, compact size, and a simple layout.

IV. CONCLUSION

In this study, a microstrip three-state switchable and fully tunable BPF was developed. An extra-wide frequency tuning range from 0.54 to 2.4 GHz—a fractional tuning range of 127%—with an approximate CABW of 82 MHz was achieved. The design idea was successfully demonstrated using full-wave EM simulation and validated using experimental results. In addition, the size of the proposed switchable and tunable BPF is only approximately $0.24\lambda_g \times 0.15\lambda_g$. Because of its extra-wide frequency tuning range, flexible frequency and bandwidth control, compact size, and simple layout, theproposed switchable and tunable BPF has potential practical applications in RF front-end communication systems.

REFERENCES

[1] Y.-H. Chun and J.-S. Hong, "Electronically reconfigurable dual-mode microstrip open-loop resonator filter," *IEEE Microw. Wireless Compon. Lett.*, vol. 18, no. 7, pp. 449–451, Jul. 2008.
[2] W. Tang and J.-S. Hong, "Varactor-tuned dual-mode bandpass filters," *IEEE Trans. Microw. Theory Techn.*, vol. 58, no. 8, pp. 2213–2219, Aug. 2010.
[3] J. Long, C. Li, W. Cui, J. Huangfu, and L. Ran, "A tunable microstrip bandpass filter with two independently adjustable transmission zeros," *IEEE Microw. Wireless Compon. Lett.*, vol. 21, no. 2, pp. 74–76, Feb. 2011.
[4] Y.-C. Chiou and G. M. Rebeiz, "A tunable three-pole 1.5–2.2-GHz bandpass filter with bandwidth and transmission zero control," *IEEE Trans. Microw. Theory Techn.*, vol. 59, no. 11, pp. 2872–2878, Nov. 2011.
[5] Y.-C. Chiou and G. M. Rebeiz, "Tunable 1.55-2.1 GHz 4-pole elliptic bandpass filter with bandwidth control and > 50 dB rejection for wireless systems," *IEEE Trans. Microw. Theory Techn.*, vol. 61, no. 1, pp. 117–124, Jan. 2013.
[6] X.-G. Wang, Y.-H. Cho, and S.-W. Yun, "A tunable combline bandpass filter loaded with series resonator," *IEEE Trans. Microw. Theory Techn.*, vol. 60, no. 6, pp. 1569–1576, Jun. 2012.
[7] P.-L. Chi, T. Yang, and T.-Y. Tsai, "A fully tunable two-pole bandpass filter," *IEEE Microw. Wireless Compon. Lett.*, vol. 25, no. 5, pp. 292–294, May 2015.
[8] H.-Y. Tsai, T.-Y. Huang, and R.-B. Wu, "Varactor-tuned compact dual-mode tunable filter with constant passband characteristics," *IEEE Trans. Compon., Package. Manuf. Technol.*, vol. 6, no. 9, pp. 1399–1407, Sep. 2016.
[9] W. Qin, J. Cai, Y.-L. Li, and J.-X. Chen, "Wideband tunable bandpass filter using optimized varactor-loaded SIRs," *IEEE Microw. Wireless Compon. Lett.*, vol. 27, no. 9, pp. 812–814, Sep. 2017.
[10] L. Gao and G. M. Rebeiz, "A 0.97–1.53-GHz tunable four-pole bandpass filter with four transmission zeroes," *IEEE Microw. Wireless Compon. Lett.*, vol. 29, no. 3, pp. 195–197, Mar. 2019.
[11] G. Zhang, Y. Xu, and X. Wang, "Compact tunable bandpass filter with wide tuning range of centre frequency and bandwidth using short coupled lines," *IEEE Access*, vol. 6, pp. 2962–2969, Dec. 2018.
[12] N. Kumar and Y. K. Singh, "Compact constant bandwidth tunable wideband BPF with second harmonic suppression," *IEEE Microw. Wireless Compon. Lett.*, vol. 26, no. 11, pp. 870–872, Nov. 2016.
[13] X. Luo, S. Sun, and R. B. Staszewski, "Tunable bandpass filter with two adjustable transmission poles and compensable coupling," *IEEE Trans. Microw. Theory Techn.*, vol. 62, no. 9, pp. 2003–2013, Sep. 2014.
[14] M. Jung and B.-W. Min, "A widely tunable compact bandpass filter based on a switched varactor-tuned resonator," *IEEE Access*, vol. 7, pp. 95178–95185, 2019.
[15] C.-F. Chen, G.-Y. Wang, and J.-J. Li, "Microstrip switchable and fully tunable bandpass filter with continuous frequency tuning range," *IEEE Microw. Wireless Compon. Lett.*, vol. 28, no. 6, pp. 500–502, Jun. 2018.
[16] F. Lin and M. Rais-Zadeh, "A tunable 0.6 GHz-1.7 GHz bandpass filter with a constant bandwidth using switchable varactor-tuned resonators," in *IEEE MTT-S Int. Microw. Symp. Dig.*, May 2015, pp. 1–4.
[17] F. Lin and M. Rais-Zadeh, "Continuously tunable 0.55-1.9-GHz bandpass filter with a constant bandwidth using switchable varactor-tuned resonators," *IEEE Trans. Microw. Theory Techn.*, vol. 65, no. 3, pp. 792–803, Mar. 2017.
[18] J. Cai, J.-X. Chen, X.-F. Zhang, Y.-J. Yang, and Z.-H. Bao, "Electrically varactor-tuned bandpass filter with constant bandwidth and self-adaptive transmission zeros," *IET Microw., Antennas Propag.*, vol. 11, no. 11, pp. 1542–1548, Sep. 2017.

[19] M. Ohira, S. Hashimoto, Z. Ma, and X. Wang, "Coupling-matrix-based systematic design of single-DC-bias-controlled microstrip higher order tunable bandpass filters with constant absolute bandwidth and transmission zeros," *IEEE Trans. Microw. Theory Techn.*, vol. 67, no. 1, pp. 118–128, Jan. 2019.
[20] A. Zakharov, S. Rozenko, and M. Ilchenko, "Varactor-tuned microstrip bandpass filter with loop hairpin and combline resonators," *IEEE Trans. Circuits Syst. II, Exp. Briefs*, vol. 66, no. 6, pp. 953–957, Jun. 2019.
[21] D. Tian, Q. Feng, and Q. Xiang, "Synthesis applied 4th-order constant absolute bandwidth frequency-agile bandpass filter with cross-coupling," *IEEE Access*, vol. 6, pp. 72287–72294, 2018.
[22] Y.-H. Cho and G. M. Rebeiz, "Tunable 4-Pole noncontiguous 0.7–2.1-GHz bandpass filters based on dual zero-value couplings," *IEEE Trans. Microw. Theory Techn.*, vol. 63, no. 5, pp. 1579–1586, May 2015.
[23] T. Yang and G. M. Rebeiz, "Tunable 1.25–2.1-GHz 4-Pole bandpass filter with intrinsic transmission zero tuning," *IEEE Trans. Microw. Theory Techn.*, vol. 63, no. 5, pp. 1569–1578, May 2015.
[24] D. Lu, X. Tang, N. S. Barker, and Y. Feng, "Single-band and switchable dual-/single-band tunable BPFs with predefined tuning range, bandwidth, and selectivity," *IEEE Trans. Microw. Theory Techn.*, vol. 66, no. 3, pp. 1215–1227, Mar. 2018.
[25] J. S. Hong and M. J. Lancaster, *Microstrip Filter for RF/Microwave Application*. New York, NY, USA: Wiley, 2001.
[26] D. M. Pozar, *Microwave Engineering*, 3rd ed. Hoboken, NJ, USA: Wiley, 2006.
[27] *M/A COM MA46H201 Data Sheet*, MACOM Technol. Solutions, Lowell, MA, USA, 2006.
[28] *Datasheet for BAR65 Series*, Infineon, Munich, Germany, 2005. [Online]. Available: http://www.infineon.com/
[29] S.-F. Chao, C.-H. Wu, Z.-M. Tsai, H. Wang, and C. H. Chen, "Electronically switchable bandpass filters using loaded stepped-impedance resonators," *IEEE Trans. Microw. Theory Techn.*, vol. 54, no. 12, pp. 4193–4201, Dec. 2006.

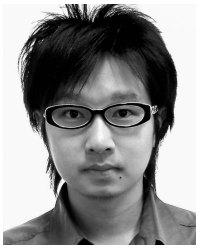

CHI-FENG CHEN (Member, IEEE) was born in Taiwan, in 1979. He received the M.S. degree in electrophysics from National Chiao Tung University, Hsinchu, Taiwan, in 2003, and the Ph.D. degree in communication engineering from National Taiwan University, Taipei, Taiwan, in 2006. From 2008 to 2010, he was an RF Engineer with Compal Communications, Inc., Taipei, where he developed global system for mobile communication (GSM) and code division multiple access (CDMA) mobile phones. In April 2010, he joined the Graduate Institute of Communication Engineering, National Taiwan University, as a Postdoctoral Research Fellow. Since 2012, he has been an Assistant Professor with the Department of Electrical Engineering, Tunghai University, Taichung, Taiwan, where he became an Associate Professor, in 2016. His research interests include the design of microwave circuits and associated RF modules for microwave and millimeter-wave applications.